Int. J. Heat Mass Transfer. Vol. 28, No. 6, pp. 1215–1227, 1985
Printed in Great Britain

0017-9310/85 $3.00 + 0.00
Pergamon Press Ltd.

Experimental and numerical study of direct contact heat exchangers

L. TADRIST, P. SEGUIN, R. SANTINI, J. PANTALONI

Laboratorie de Dynamique et Thermophysique des Fluides, Université de Provence, rue H. Poincaré, 13397 Marseille Cedex 13, France

and

A. BRICARD

Centre d'Etudes Nucléaires de Grenoble, Service des Transferts Thermiques 85X 38041 Grenoble Cedex, France.

(*Received* 11 *September* 1984)

Abstract—This paper is a study of a direct contact heat exchanger with a liquid–solid transition. The experiments were carried out on two systems at different working temperatures: Hitec/oil (at 140°C) paradichlorobenzene/water (at 50°C). The particle size distribution at the exchanger column outlet is a function of dispersed-phase and continuous-phase temperatures as well as of the relative velocity of the two fluids at the nozzle. We have established a model based on the heat transfer characteristic times: There is a correlation between the heat exchanger efficiency to the characteristic Peclet number of this type of heat exchangers. We established another model of the heat transfer inside the two-phase flow, giving the temperature profile of the continuous phase along the exchange column and the efficiency of the heat exchange. The results of this model were compared to those obtained experimentally.

INTRODUCTION

DIRECT contact heat exchangers occupy an important place in the field of research and development of new types of heat exchanger. Their working principle is similar to that of chemical reactors. This direct contact has many advantages compared to conventional heat exchangers. There is a large, free heat transfer surface associated with the possible change of state of the two fluids. This process is particularly suited to latent heat storage systems, industrial waste heat recovery systems or geothermal systems.

The principle of these exchangers is to allow intimate contact between a hot fluid ϕ_1 and cold fluid ϕ_2. The mixing technique used determines the type of heat exchanger: 'layer heat exchanger' or 'spray heat exchanger'.

In the layer exchanger [1, 2], the fluid ϕ_1 is stagnant while ϕ_2 flows on top. The interface defines the heat transfer surface and the developing surface instabilities have an important effect on the heat transfer [1]. In the spray type, one of the fluids is dispersed in the other. The dispersion may be done in two ways: in the integrated type exchanger the fluid ϕ_2 is pumped through the fluid ϕ_1 [Fig. 1(a)] while in the split type exchanger the fluid ϕ_1 is injected into the flowing fluid ϕ_2 [Fig. 1(b)]. The latter type has been particularly studied in liquid–liquid systems for sea water desalination plants [4, 5] and for industrial exchangers [6]. Because of the absence of solid walls between the fluids there are none of the problems associated with heat transfer surfaces such as corrosion or scaling. The split type exchanger is particularly advantageous when a change of state occurs [7] (solidification or vaporization of one or both of the two fluids). Table 1 gives the possible exchange combinations associated with the different kinds of change of state.

The purpose of this paper is to study the split type direct contact heat exchangers where a hot fluid ϕ_1 is

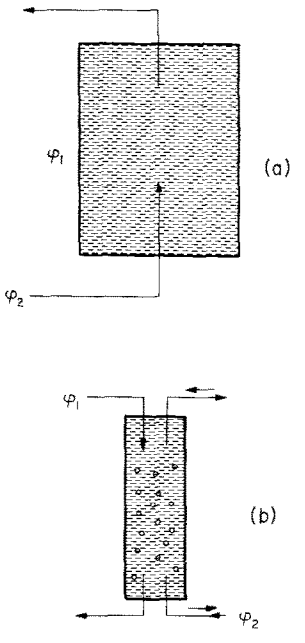

FIG. 1. Schematic of spray type heat exchanger: (a) integrated type heat exchanger, the heat carrier fluid ϕ_2 is directly injected into the hot stock contained in tank 1; (b) split type heat exchanger: the heat storage fluid ϕ_1 is directly injected into the co-current or counter-current flowing heat carrier fluid ϕ_2.

NOMENCLATURE

A, B coefficients defined in the law $\langle X \rangle$ vs v_r
Bi Biot number
C specific heat
C_x drag coefficient
dt residence time of the particle in the thickness dz of the column
D exchanger column diameter
d nozzle diameter
d_{32} Sauter diameter
$\dot{E}x$ exergy flow rate
Een exergetic efficiency
g acceleration due to gravity
H enthalpy function
h_v volumetric heat transfer coefficient
h local heat transfer coefficient at the interface of the continuous and dispersed phase
E exchanger efficiency
L exchanger height
L_f latent heat of fusion of dispersed phase
m_i mass percentage recovered at each sieve
m_k mass percentage of particles of diameter X_k
$\dot{m}$ mass flow rate
M distribution function associated with the log-normal law
Nu_p particle Nusselt number
p log-normal function
P_{ec} transferred heat flow rate
P_f maximum transferable heat flow rate
Pe' modified Peclet number
Pr Prandtl number
R^* radius of solidification front
R external radius of particle
Re_p Reynolds number of particle
Re_c continuous phase Reynolds number
r, t space–time coordinates
T temperature
T_{di} dispersed phase temperature at $z = 0$
T_{ce} continuous phase temperature at $z = 0$
T_p temperature of fusion
T_{cs} continuous phase outlet temperature
T_{cl} equilibrium temperature of the two phases
u adimensionned solidification radius
U_R relative velocity of particle
U_R^∞ relative velocity of a single particle in the continuous phase
V_c continuous phase absolute velocity
V_i nozzle jet velocity
V_r relative velocity of injection
v_d absolute velocity of particle
X particle diameter
X_i sieve mesh size
$\langle X \rangle$ mass average diameter
z exchanger column abscissa.

Greek symbols
α dispersed phase fraction
ε parameter = 1 in co-current regime
= −1 in counter-current regime
ξ, η log-normal function parameters
θ_0 reference temperature
λ thermal conductivity
ν kinematic viscosity
ρ density
σ standard deviation
σ_i surface tension
τ_s particle residence time in the exchanger
τ_{th} characteristic time of heat transfer from particle to continuous phase
ψ volumetric flow rate
Ω column cross section.

Subscripts
p particle
c continuous phase
d dispersed phase
k particle group collected in each sieve
dl dispersed-phase liquid
ds dispersed-phase solid.

Superscripts
∞ single particle in an infinite medium at rest.

Table 1. Possible exchange combination associated with different kinds of change of state

Fluid ϕ_1	Fluid ϕ_2
Liquid–solid	Liquid
Liquid–solid	Gas
Liquid–gas	Liquid
Liquid–solid	Liquid–gas

injected into a cold fluid ϕ_2 accompanied with a liquid–solid change of state of the fluid ϕ_1. The drops issuing from the breaking of the fluid jet ϕ_1 solidify while flowing. Heat transfer to the fluid ϕ_2 takes place at a constant temperature. This advantage is non-existent in conventional heat exchangers because of the formation of a solid crust on the exchanger walls which decreases the heat flow rate [8–11]. Despite these

undeniable advantages, development of this type of heat exchanger is limited by some disadvantages. They require suitable couples ϕ_1/ϕ_2 which are immiscible and chemically inert. Moreover, the separation of the two phases at the heat exchanger outlet complicates the system because a separation technique must be used (centrifuge, Archimedean screw).

Preliminary studies carried out on the couple: ϕ_1(NaCl)/ϕ_2(Na) showed the feasibility of the process despite the important solubility phenomenon [12]. A second couple has been tested: ϕ_1 (eutectic mixture NaCl–$CaCl_2$)/ϕ_2 (Na). This system presents chemical reaction and solubility phenomena [13]. As the initial products were not integrally recovered over an exchange cycle because of the latter inconveniences, this study showed that direct contact is not adapted when these phenomena are present.

Therefore two couples which are chemically non-reactive and insoluble, and whose working temperatures allow the observation of the exchange process through the glass apparatus, were used.

ϕ_1 : eutectic mixture $NaNO_3$–KNO_3–$NaNO_2$/ϕ_2 : organic oil [14]

ϕ_1 : paradichlorobenzene ($C_6H_4Cl_2$)/ϕ_2 : water [15, 16].

They gave rise to two experimental set-ups.

General laws governing these heat exchangers and leading to their modelization and to the elaboration of computational codes can be established from the results obtained.

APPARATUSES AND PROCEDURE

A schematic diagram of the apparatus coupled with an energy storage system is shown in Fig. 2. The liquid phase ϕ_1 contained in tank 1 is injected at constant temperature into the flowing phase ϕ_2. The direct contact heat transfer takes place in the exchanger 2 thereby freezing the phase change material droplets issuing from the jet break-up. The extracted solid particles are stored in tank 3. The phase change material ϕ_1 contained in the storage system is brought back to the liquid state by a heat supply. The different nature of the two couples and their working temperatures led us to develop two separate types of apparatus: One for a molten salt (Hitec/oil), the other for an organic material (paradichlorobenzene/water).

Molten salt system

The phase change material ϕ_1 is an eutectic mixture of mineral salts whose mass percentages are KNO_3 50%, $NaNO_3$ 7%, $NaNO_2$ 43% (m.p. 142°C). The phase ϕ_2 is a synthetic organic oil. The heat exchanger is a cylindrical column, thermally insulated, of length L = 100 cm and diameter D = 8 cm. A cylindrical pipe of length L = 20 cm and diameter d = 0.4 cm allows the dispersion of phase ϕ_1 into phase ϕ_2. Heat flow rate in the exchanger varies between 2 and 17 kW.

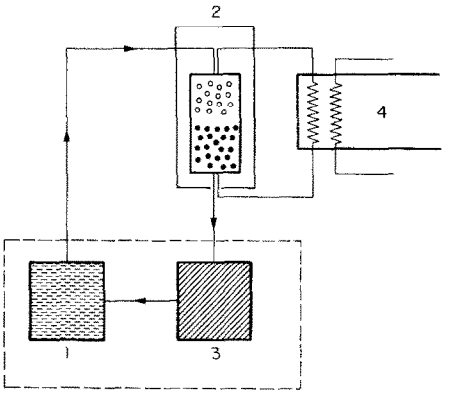

FIG. 2. Block diagram of heat storage–heat exchanger–secondary heat exchanger system: (1) liquid heat storage material tank; (2) direct contact heat exchanger; (3) solid heat storage material tank; (4) secondary heat exchanger (utilization circuit).

Organic fluid system

The phase change material ϕ_1 is an organic compound: $C_6H_4Cl_2$ (m.p. 53°C). The continuous phase ϕ_2 is water. The heat exchanger is a cylindrical column, non-insulated because of the low working temperature, maximum heat loss was evaluated at 3%, the phase change material percolated through 18 holes (0.07 cm diameter) in the distribution plate. Heat flow rate in the exchanger was of the order of 5 kW.

The system can be operated either for heat storage, or continuously, as a three fluid heat exchanger. The phase change material ϕ_1 is then used as intermediary between a hot fluid (source) and a secondary fluid (utilization).

Rotameters with analog displays were used to measure the flow rates (error less than 5%). Temperatures were measured with chromel–alumel thermocouples. The dispersed phase ϕ_1 temperature was taken at the injector inlet while the phase ϕ_2 inlet and outlet temperatures were measured in the exchanger. Moreover, temperatures along the cylindrical column were taken in the paradichlorobenzene/water exchanger. Temperature readings were correct to 0.5°C.

EXPERIMENTAL RESULTS

Heat transfer in the exchanger column between the dispersed phase and continuous phase is closely related to the nature of the flow. Two distinguishable flow zones were noticed:

—Drop formation and deceleration zone.
—Dilute dispersion flow zone, where the drops occupy the column cross-section with homogeneous concentration.

The characteristic parameters of the system's hydrodynamics and the drop thermal states are functions of the particle size resulting from the injection conditions.

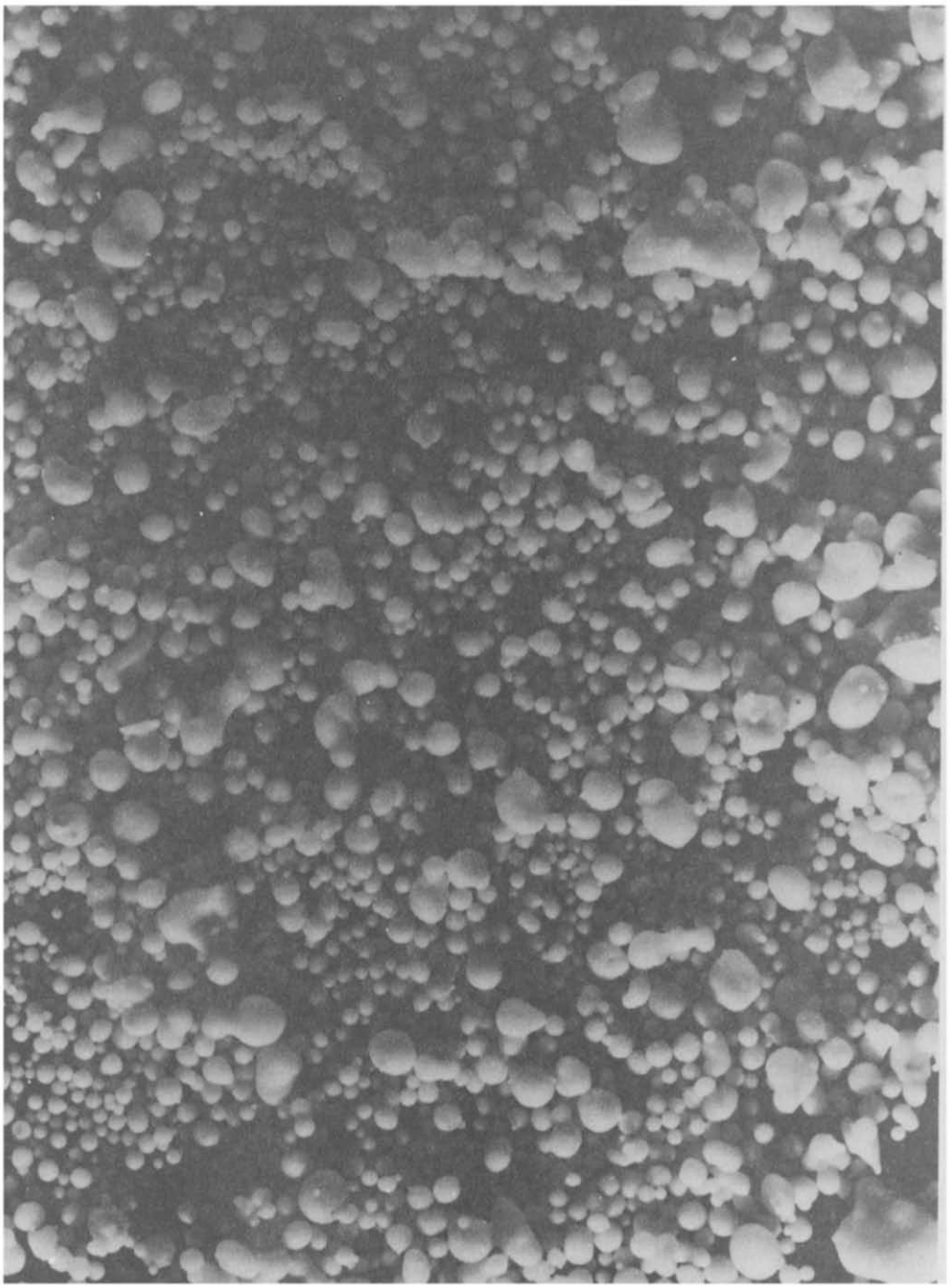

FIG. 3. Example of Hitec particles obtained at the Hitec/oil exchanger outlet, particles size varies from 1 to 5 mm.

Analysis of the particle size

Figure 3 gives some examples of particle shapes obtained. After each injection solid particles, sampled and sifted, were classified according to their size. The mass percentage histogram of each group size was obtained. We associate with this histogram the mean diameter:

$$\langle X\rangle = \sum_{i=1}^{n-1} \frac{X_i + X_{i+1}}{2} m_i + X_n m_n \qquad (1)$$

and the standard deviation:

$$\sigma = \left\{ \sum_{i=1}^{n-1} \left(\frac{X_i + X_{i+1}}{2} - \langle X\rangle \right)^2 m_i + (X_n - \langle X\rangle)^2 m_n \right\}. \qquad (2)$$

In heat transfer problems, it is important to make use of the greatest heat transfer surface for a given volume, therefore a characteristic diameter is used: the Sauter

diameter [17] is defined as:

$$d_{32} = \frac{\sum_{i=1}^{n-1} \left(\frac{X_i + X_{i+1}}{2}\right)^3 m_i + X_n^3 m_n}{\sum_{i=1}^{n-1} \left(\frac{X_i + X_{i+1}}{2}\right)^2 m_i + X_n^2 m_n}. \quad (3)$$

The analysis of the experimental results require knowledge of the probability law governing the particle size distribution. Epstein [18] basing his arguments on probabilistic considerations, suggested the use of a log-normal distribution:

$$p(X) = C \exp[-(\log X - \eta)^2 / 2\xi^2] \quad (4)$$

where C is a normalization constant:

$$C = \frac{1}{\xi\sqrt{2\pi}} \exp -(\eta + \tfrac{3}{2}\xi^2).$$

Mean size and standard deviation are given by:

$$\langle X \rangle = \exp(\eta + \tfrac{3}{2}\xi^2) \quad (5)$$

$$\sigma = \exp(2\eta + 3\xi^2) \exp(\xi^2 - 1). \quad (6)$$

Figure 4 shows a close agreement between the experimental points and the log-normal distribution. Maximum deviation between experimental values of $(\langle X \rangle, \sigma)$ and those given by equations (5) and (6) are 4% and 20% respectively. The error in standard deviation becomes more significant as the mean size increases ($\langle X \rangle > 4$ mm). In this case the measurement technique is less reliable due to the irregular shape of the particles.

Effect of injection conditions on particle size distribution

The particle size distribution obtained at the exchanger outlet results from a multiple stages process:

—drop formation from one or more jets;
—drop evolution by break-up and coalescence;
—solidification, stopping this evolution.

Any change in the latter stages induces a variation in particle size distribution. A complete study must therefore take account of all the characteristic properties likely to influence the hydrodynamic and thermal processes. The size distribution of particles collected at the exchanger outlet is a function of the following properties:

$$p(x) = f(v_d, v_c, \rho_c, \rho_d, \sigma_i, d, D, V_c, V_i, T_c, T_d, T_f)$$

Physical considerations led us to take combinations of the various variables:

—Jet break-up is mainly governed by interfacial shear and therefore by the relative velocity of the two fluids $V_r = V_i - V_c$.
—Drop coalescence and break-up probabilities are functions of the dispersed phase concentration.
—Freezing, which stops size evolution, is blocked by the temperature differences $\Delta T_d = T_d - T_f$ and $\Delta T_c = T_f - T_c$.

For a given prototype (fixed geometry and given couple) several of these variables remain constant, the particle size distribution is then given by:

$$p(X) = g(v_d(T_d), v_c(T_c), V_r, \alpha(V_c, V_i), \Delta T_d, \Delta T_c).$$

This equation is still complex and only an experimental approach reveals the relative influences of the various parameters on mean size $\langle X \rangle$ and standard deviation σ.

The results for $\langle X \rangle$ and σ relating to the paradichlorobenzene/water pair were not numerous enough to identify any correlation existing between these parameters and the latter properties. Figure 5 shows the evolution of Sauter diameter vs the relative velocity of injection for several temperature difference ratios $(\Delta T_c/\Delta T_d)$. It can be observed that the dispersed phase change of state amplifies the particle coalescence phenomenon. At low relative velocities of injection ($V_r < 2$ m s^{-1}) the mean diameter is greater than that obtained by Christiansen and Hixon correlation [19] for liquid–liquid spray columns, and is strongly dependant on temperature conditions. At higher relative velocities of injection, ($V_r > 2$ m s^{-1}), the T_c and

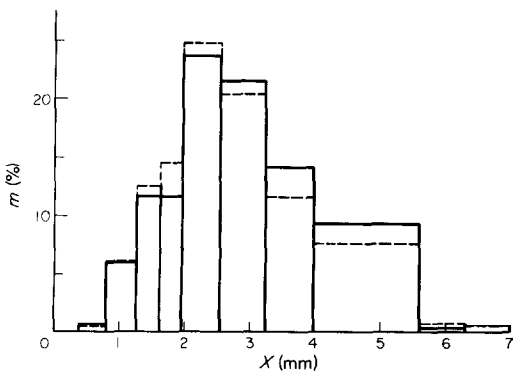

FIG. 4. Particles size histogram over an exchange cycle (Hitec/oil couple): ——— experimental histogram; ---- histogram given by the log-normal distribution.

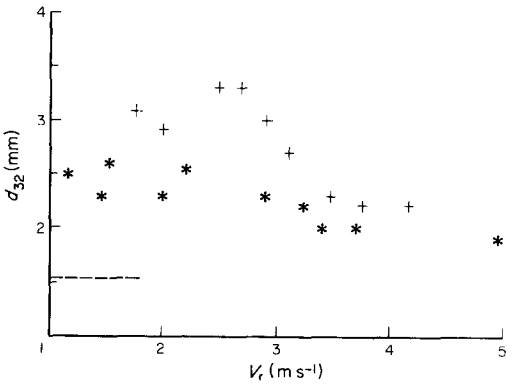

FIG. 5. Sauter diameter vs the relative velocity of injection (paradichlorobenzene/water pair): +, $0.4 < \Delta T_c/\Delta T_d < 0.8$; *, $\Delta T_c/\Delta T_d > 0.8$; ----, Christiansen and Hixon correlation in liquid–liquid systems.

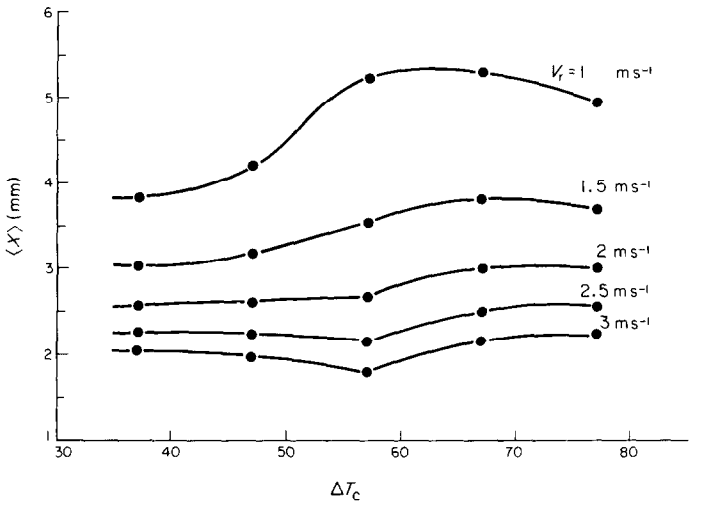

FIG. 6. Variation of the mean diameter $\langle X \rangle$ vs ΔT_c for different relative velocities of injection (Hitec/oil pair).

T_d temperatures have no significant influence on the drop size distribution.

Figure 6 shows $\langle X \rangle$ vs ΔT_c for the Hitec/oil piar and for five relative velocities of injection V_r. This array of curves clearly shows that if the temperature difference ΔT_c is fixed, variation in velocity has a significant effect on the value of the mean diameter. On the other hand, if the relative velocity of injection is fixed (isovelocity curve), variations in the temperature difference are significant only at lower velocities. These considerations led us to search for a relation $\langle X \rangle = f(V_r)$. Although many authors who have studied liquid–liquid system granulometry [19, 20] have not taken account of the freezing phenomenon, we, like Putnam [20] have considered a function of the form $\langle X \rangle = AV_r^{-B}$; our experimental results are in close agreement with this law as shown in Fig. 7. The coefficients A and B depend on the thermophysical properties of the fluid and must therefore be determined for each pair used.

Efficiency of the heat exchanger

The heat exchange between the two materials is not total because the solid crust formation around every particle prevents complete heat transfer. The exchanger efficiency is thus defined as the ratio of the transferred heat flow rate to the maximum heat flow rate:

$$E = \frac{\int_{T_{ce}}^{T_{cs}} C_c \, dT}{\int_{T_{ce}}^{T_{cl}} C_c \, dT}$$

where T_{cl} is the thermal equilibrium temperature of the two materials.

Exchanger efficiency appears to be closely related to the mean diameter of the particles (Fig. 8). This parameter conditions both the solid crust thickness and the terminal velocity of the particles. Therefore, we define two characteristic times:

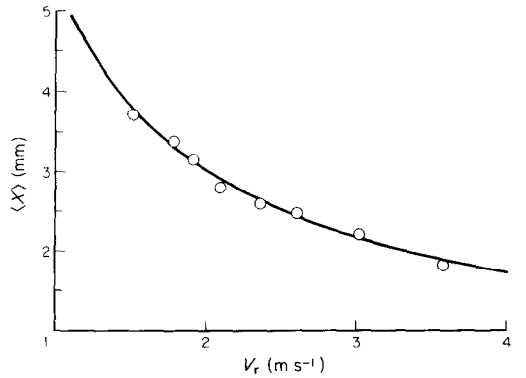

FIG. 7. Variation of particles mean diameter $\langle X \rangle$ vs the relative velocity of injection for $\Delta T_c = 67°C$ (Hitec/oil couple in co-current flow): ○, experimental points; ——, curve given by the equation $\langle X \rangle = 5.32\ V_r^{-0.815}$.

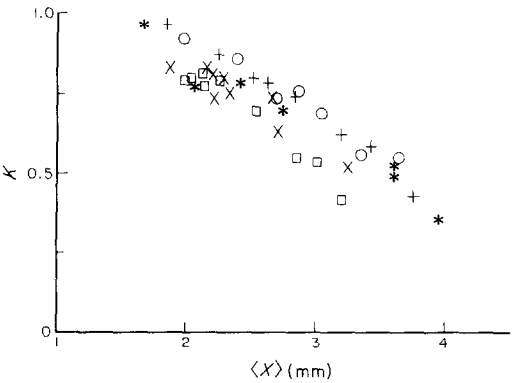

FIG. 8. Variation of exchanger efficiency E vs $\langle X \rangle$ for different ΔT_c (Hitec/oil couple in co-current flow): ○, $\Delta T_c = 77°C$; +, 67°C; *, 57°C; × = 47°C; □, 37°C.

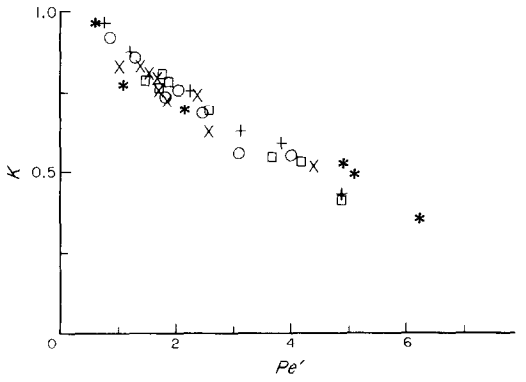

FIG. 9. Variation of the efficiency coefficient E vs the Peclet number (Hitec/oil couple in co-current flow): ○, $\Delta T_c = 77°C$; +, 67°C; *, 57°C; ×, 47°C; □, 37°C.

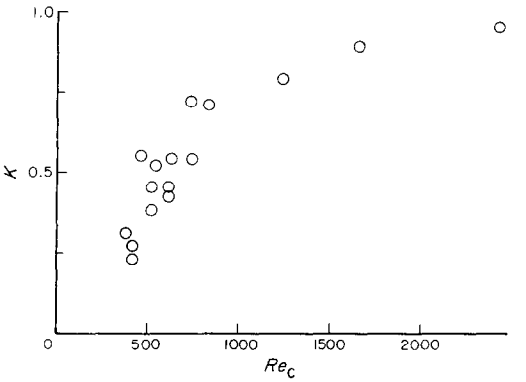

FIG. 10. Variation of the efficiency E vs the continuous phase Reynolds number Re_c (paradichlorobenzene/water): $d_{32} <$ 2.5 mm, $20 < T_{ce} < 30°C$.

τ_s: particle residence time in the exchanger,

τ_{th}: thermal transfer time between the particle and continuous phase.

The ratio residence to thermal transfer time defines the Peclet number characterizing this type of heat exchanger. τ_s and τ_{th} can be calculated using a simplified transfer model [21] thus leading to the following expression for the Peclet number:

$$Pe = \frac{\langle X\rangle^2 P_f V_d}{12 L \lambda_d \psi_d [T_d(0) - T_c(L)]}. \quad (7)$$

The study of exchanger efficiency as a function of the Peclet number defined above shows a close correlation between these quantities (Fig. 9) expressed by the following relation:

$$E = \alpha_1 Pe^{\beta_1}.$$

The operation of the heat exchanger is defined aggregately by the Peclet number and the mean diameter, which is deduced from the expression $\langle X\rangle = A V_r^{-B}$. However, the expression (7) doesn't account for all the observed phenomena, especially the increasing efficiency with increasing continuous phase flow rate in counter-current flow. Independently of the heat exchange parameters (h, α, ΔT, d_{32}) which didn't vary significantly at a constant dispersed flow rate, this increase suggests a better heat transfer related to the hydrodynamic regime in the column, which is characterized by the Reynolds number $Re_c = V_c D/\nu_c$ (Fig. 10).

Exergetic efficiency

In a complete study of the heat exchanger, it is necessary to evaluate its exergetic efficiency [33]. The latter takes account of the exergy destructions in the heat exchanger.

In the case of direct contact heat exchangers, these energy destructions are mainly due to thermal irreversibilities [14]. Exergetic is defined as the ratio of the exergy recovered by the 'cold' fluid to that given by the 'hot' fluid:

$$Een = \Delta \dot{E}x_c / \Delta \dot{E}x_d.$$

This efficiency varies between 30% and 75% in our experiments and no significant difference was observed between co-current and counter-current flows.

In the $[1-(\theta_0/T), H]$ plane (Fig. 14), the representation of the heat exchanger thermodynamic transformation shows that the area between AA' and BB' corresponds to the exergy destroyed. The presence of the plateau corresponding to the change of state of dispersed phase necessarily implies the destruction of exergy. This destruction can be minimized by balancing the heat fluxes of the two materials.

For heat exchanger efficiency higher than 95% and holdup of the order 5% the volumetric heat transfer coefficients are of the order of 100 kW m^{-3} °C^{-1} for the Hitec/oil exchanger and 45 kW m^{-3} °C^{-1} for the paradichlorobenzene/water exchanger.

These values are higher than those obtained for the liquid–liquid heat exchanger given by the following correlations [22] for oil/water systems:

$$h_v \text{ (kW m}^{-3}\text{ °C}^{-1}) = 223\alpha \quad \text{for} \quad \alpha \leqslant 5\%.$$

COMPUTATIONAL ANALYSIS

In this section an analysis is developed to determine the influence of various parameters (geometric, hydrodynamic and thermal) on dispersed phase and continuous phase temperature profile. A completely theoretical approach is not possible. Therefore it is necessary to establish models that take account of the physical aspects of the problem. Similar studies have been done on analog systems [23, 24] but the results obtained cannot be extended to the direct contact heat exchanger: ϕ_1 (liquid–solid)/ϕ_2 (liquid). We propose two numerical methods which allow the resolution of this problem.

Hydrodynamic approach

The system is assumed to be a flow of known particle distribution in a flowing liquid. The two-phase flow is supposed mono-dimensional with uniform holdup. Size distribution induces an absolute velocity distribution of the particles:

$$v_{dk} = U_{rk} + \varepsilon V_c. \tag{8}$$

Variation of holdup (1.5% to 6%) modifies the drag coefficient and therefore the terminal relative velocity, which is expressed for a single particle in a stagnant infinite medium as:

$$U_{Rk}^{\infty} = \left[\frac{4(\rho_d - \rho_c)X_k}{3\rho_c C_{xk}^{\infty}}\right]^{1/2}. \tag{9}$$

For holdup more than 3%, the mean drag coefficient can be estimated using Ergun's equation [25], which characterizes the pressure drop across a bed of particles:

$$C_{xk} = \frac{7}{3(1-\alpha)} + \frac{200\alpha}{(1-\alpha)^2 Re\, p_k} \tag{10}$$

with

$$\alpha = \psi_d/[\Omega U_R + \varepsilon\psi_c/(1-\alpha)]. \tag{11}$$

Iterative computations on the relations (9)–(11), where $X_k = d_{32}$ determines the holdup. The relative velocity for each class of particles was calculated from equations (8) and (9). For holdup less than 3% it is supposed that interaction between the particles is negligible. In this case the relative velocity is expressed by using the following correlation for the drag coefficient:

$$C_{xk}^{\infty} = 18.5(Re_{pk}^{\infty})^{-0.6}. \tag{12}$$

Moreover the holdup can be calculated from the Richardson and Zaki correlation [26]:

$$U_R = U_R^{\infty}(1-\alpha)^{n-1} = \frac{\psi_d}{\alpha\Omega} + \frac{\psi_c}{(1-\alpha)\Omega}$$

where

$$n = 4.45\, Re_p^{\infty\,-0.1} \quad \text{for} \quad 1 < Re_p^{\infty} < 500.$$

Thermal approach

In order to maintain the mathematical tractability of the problem a number of simplifying assumptions were used: the drop shape is assumed spherical and the temperature distribution in the drop is assumed to have a spherical symmetry.

Heat transfer in the particle is governed by the following equations:

—Heat conduction:

$$\rho_c c_d(T_d)\frac{\partial}{\partial t}T_d(r,t) = \frac{\lambda_d}{r}\frac{\partial^2}{\partial r^2} r T_d(r,t). \tag{13}$$

—Heat balance at freezing front:

$$\rho_d L_f \frac{d}{dt}R^* + \lambda_{dl}\frac{\partial}{\partial r}T_{dl}(r,t)\bigg|_{r=R^*} = \lambda_{dl}\frac{\partial}{\partial r}T_{ds}(r,t)\bigg|_{r=R^*}. \tag{14}$$

—Heat flux at liquid–particle interface:

$$\lambda_d \frac{\partial}{\partial r}T_d\bigg|_{r=R_k} = h_k(T_d(R_k,t) - T_c). \tag{15}$$

—Temperature at freezing front:

$$T_d(R^*,t) = T_f. \tag{16}$$

Because equation (14) is not linear, analytical integration of the preceding system of equations is not feasible and only numerical integration is possible; several methods are proposed [24, 27]. In the present work two methods will be developed: The enthalpic method [15] and the stationary method [14].

(1) In the enthalpic method, we consider an enthalpy function H, equation (14) can thus be neglected and the system of equations linearized. Moreover, heat transfer in the drop is considered conductive. The final freezing radius is given by:

$$R_f^* = R_k\left(\frac{\rho_{ds} - \rho_{dl}}{\rho_{ds}}\right)^{1/3}. \tag{17}$$

Thermal drop profile is calculated from:

$$\rho_d r^2(z) v_k \frac{d}{dz}H(T) = \lambda_d \frac{\partial}{\partial r}\left[r^2(z)\frac{\partial T}{\partial r}\right] \tag{18}$$

where

$$dz = v_k\, dt$$

with the boundary condition:

$$\lambda_d \frac{\partial T}{\partial r}\bigg|_{r=R_k} = h_k[T_d(R_k,z) - T_c(z)]. \tag{19}$$

It is possible to determine the temperature from the enthalpy diagram $H = f(T)$ due to the local evolution of the enthalpy function between the abscissa z and $z+dz$.

Therefore the problem is solved by the integration of the local heat balance equation:

$$\varepsilon\rho_c C_c \psi_c \frac{\partial}{\partial z}T(z) = \sum_{k=1}^{n}\frac{6\psi_d m_k h_k}{X_k v_{dk}}[T_d(R_k,z) - T_c(z)] \tag{20}$$

with the temperature boundary conditions at the injector:

$$T_d(R_k,0) = T_{di} \quad \text{and} \quad T_c(0) = T_{ce} \tag{21}$$

(2) In the stationary method we resolve the transfer into three stages:

—heat transfer in the drop at uniform temperature down to the melting point;
—latent heat transfer with a temperature profile in the crust corresponding to the stationary case (the particle freezes in giving up only its latent heat), until the freezing radius equals R_f^*; and
—heat transfer in the solid particle at uniform temperature.

The system of equations governing the heat transfer is:

$$\frac{\mathrm{d}}{\mathrm{d}z} T_{dk}(z) = \frac{6h_k}{v_{dk} X_k C_d \rho_d} [T_c(z) - T_{dk}(z)] \quad (22)$$

$$\frac{\mathrm{d}}{\mathrm{d}z} U_k = \frac{2h_k}{X_k \rho_d L_f v_{dk} U_k^2} \frac{T_c(z) - T_f}{1 + \frac{Bi_k}{2}\left(\frac{1}{U_k} - 1\right)} \quad (23)$$

where

$$U_k = R^*/R_k \quad \text{and} \quad Bi_k = \frac{h_k X_k}{\lambda_k}.$$

Heat balance of a unit volume is expressed by:

$$\varepsilon \rho_c C_c \psi_c \frac{\mathrm{d}}{\mathrm{d}z} T_c(z) = \sum_{k=1}^{k=j} \frac{1}{X_k v_{dk}} 6\psi_d m_k h_k \times [T_{dk}(z) - T_c(z)] + \sum_{k=m+1}^{k=p} \frac{1}{X_k v_{dk}} \times 6\psi_d m_k h_k [T_{dk}(z) - T_c(z)] + \sum_{k=j+1}^{k=m} \frac{1}{X_k v_{dk}} 6\psi_d m_k h_k \frac{T_f - T_c(z)}{1 + \frac{Bi_k}{2}\left(\frac{1}{U_k} - 1\right)}. \quad (24)$$

For both methods, modelization of the thermal transfer implies the choice of an appropriate correlation for the adimensioned convection heat transfer coefficient given by the Nusselt number:

$$Nu = a + b\, Re_p^c\, Pr_c^{1/3}.$$

The coefficients a, b and c can be determined according to the flow regime by numerous experimental and numerical studies. Among the proposed correlations Rowe's equation [28] relative to a fixed sphere in mono-dimensional flow is used. This correlation is valid for two-phase flow at low holdup ($\alpha < 3\%$):

$$Nu_p = 2 + 0.79\, Re_p^{1/2}\, Pr_c^{1/3}. \quad (25)$$

At large concentration where the spheres interact, Chu [29] proposes:

$$Nu_p = 1.77\alpha^{0.44}\, Re_p^{0.56}\, Pr_c^{1/3}. \quad (26)$$

The dispersed-phase temperature for each class of particles and the continuous-phase temperature profile along the exchanger column were obtained by solving each system of equations using the method of finite differences.

COMPARISON OF COMPUTATIONAL AND EXPERIMENTAL RESULTS

Comparison

For co-current flow, experimental and computational temperature profiles and exchanger efficiencies are in close agreement for any two-phase flow regime (Fig. 11, Table 2). Relative deviation between the experimental and computational results is about 5%.

On the other hand, for counter-current flow there is little agreement between measured continuous-phase temperatures and those given by the computations (Fig. 12), which overestimate the exchanger efficiency. However, the deviation between experimental and computational exchanger efficiencies decreases with increasing continuous flow rate.

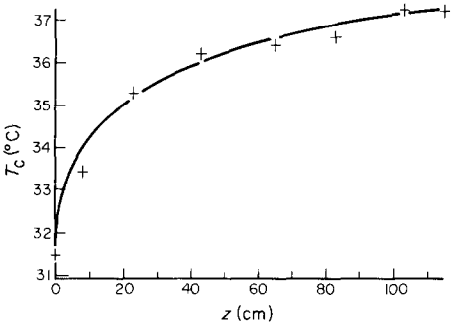

FIG. 11. Continuous-phase temperature profile $T_c(z)$ along the exchanger in co-current flow (paradichlorobenzene/water exchanger). Zero point is chosen at the injector: +, experimental points; ———, simulation results: the two models given the same result. $\psi_d = 14.89$ cm s^{-1}, $\psi_c = 111.11$ cm^3 s^{-1}.

For counter-current flow, the continuous-phase temperature profile is characterized by a seizing of heat transfer in the injection zone, even for efficiencies much lower than unity, while for co-current flow the exchanged heat flux is maximum.

Analysis

In the preceding computational models we assume a uniform dispersed phase distribution in a cross section at every point of the column. Complex phenomena such as entrance and exit effects, wall effects and injection effects which cannot be isolated, and which induce velocity heterogeneity, are not considered in the models. These phenomena, typical of spray systems are known as axial dispersion [6, 30–32]. Models using a dispersion coefficient that depends on the nature of the fluids were proposed to describe the deviation from a homogeneous flow in counter-current liquid–liquid dispersions and in fluidized beds. This coefficient adjusts the computed temperature profile to the

Table 2. Experimental and numerical efficiencies obtained for different continuous and dispersed flow rates in co-current flow (paradichlorobenzene/water couple)

ψ_d (cm^3 s^{-1})	ψ_c (cm^3 s^{-1})	E (experimental) (%)	E (estimated) (%)
22.22	408.33	56.5	56.3
25.00	666.66	62.6	62.6
27.22	694.44	74.3	66.7
30.55	666.66	78.2	73.3
33.61	666.66	76.9	75.4
35.83	694.44	80.9	79.6
39.72	666.66	78.8	80.4
42.50	666.66	83.3	85.5
45.27	408.33	92.3	88.5

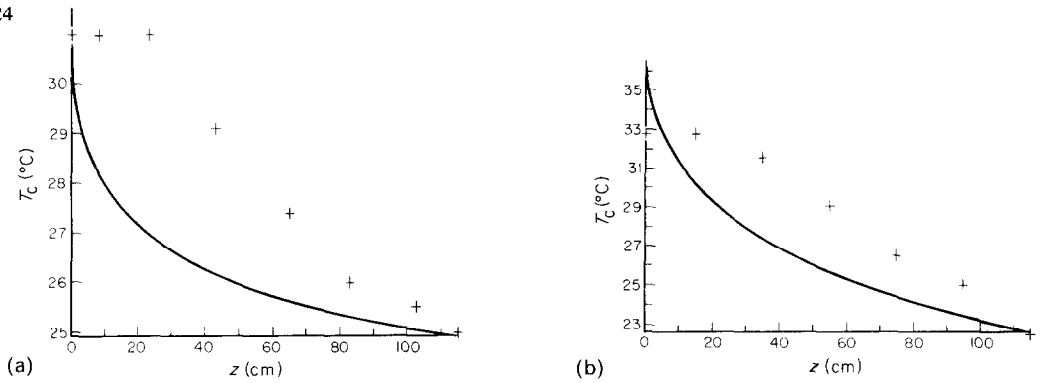

FIG. 12. Continuous-phase temperature profile $T_c(z)$ along the exchanger in counter-current flow (paradichlorobenzene/water exchanger): (a) $\psi_d = 13.89$ cm^3 s^{-1}, $\psi_c = 41.67$ cm^3 s^{-1}, E(experimental) = 92%, E(estimated) = 95%; (b) $\psi_d = 13.89$ cm^3 s^{-1}, $\psi_c = 111.11$ cm^3 s^{-1}, E(experimental) = 92%, E(estimated) = 97%.

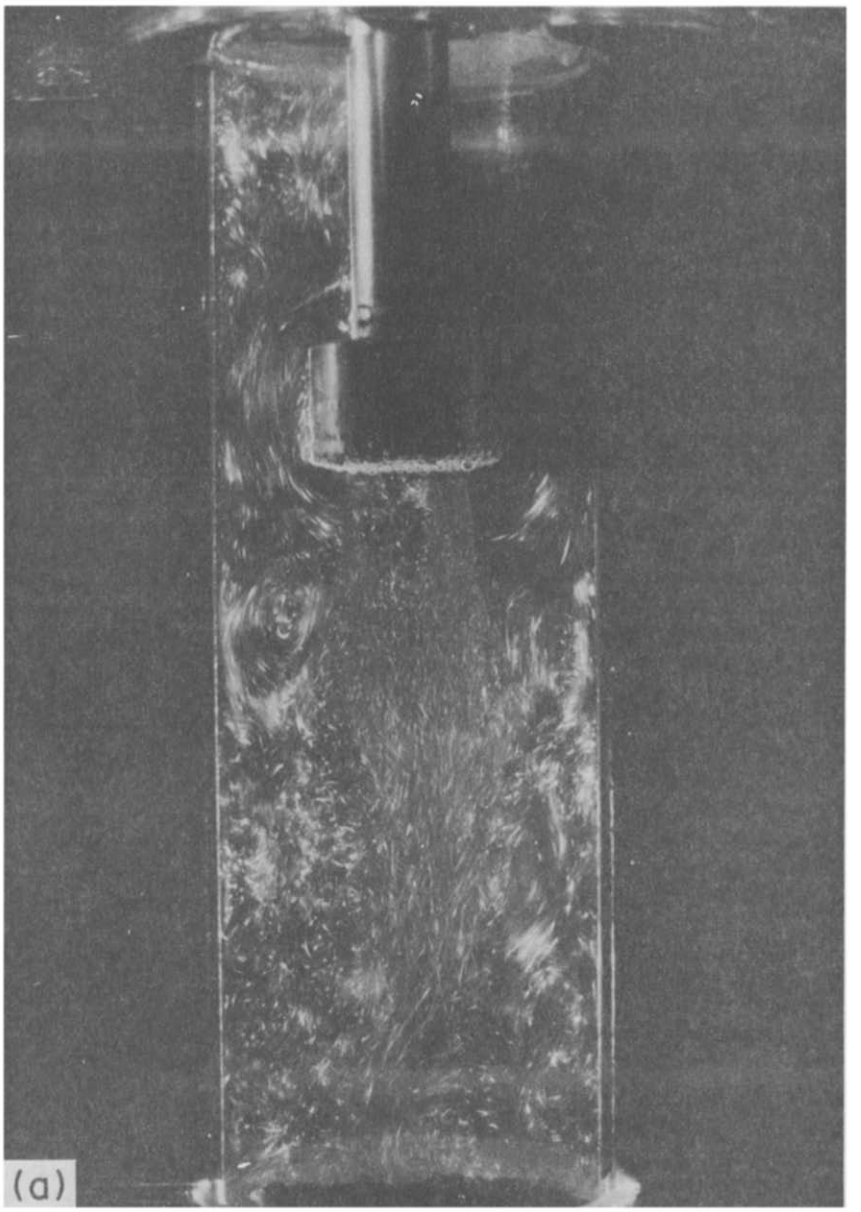

FIG. 13(a).

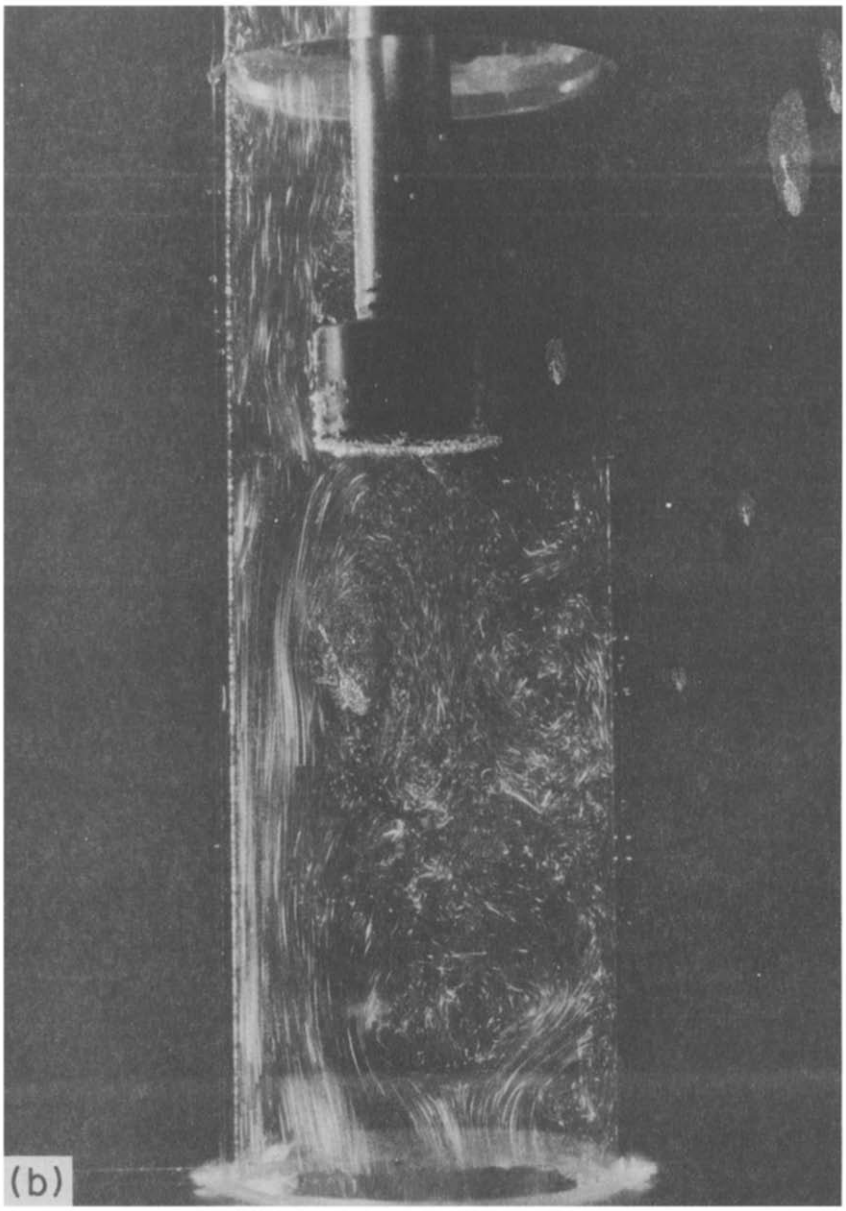

FIG. 13. Visualization of the liquid injection in a liquid–liquid system (paradichlorobenzene/water exchanger): (a) co-current flow; (b) counter-current flow.

experimental temperature profile in some specific cases. Analysis of previous works and our experiments show that the origin of the discrepancies between co- and counter-current results is hydrodynamic, especially at the injection zone.

Visualization experiments with a high slit were carried out on the paradichlorobenzene/water heat exchanger. They show that the mixing process of the two phases at the injection zone is quite different according to the flow mode (Fig. 13). In co-current flow the continuous phase already disturbed by the injector is sucked in by the injected phase. It follows a high mixing all along the column [Fig. 13(a)]. This results in a homogeneous distribution of the dispersed phase in the continuous phase. In this case an homogeneous flow assumption corresponds to the physical reality.

On the other hand in the counter-current regime the two-phase flow is quite different. It can be observed that the continuous phase has specific trajectories; it results in a non-homogeneity of the distribution of the two phases in the column [Fig. 13(b)] thus explaining why models that assume a homogeneous distribution of the dispersed phase do not agree with the experimental results. Moreover, the continuous-phase temperature measured at a given point in the exchanger column is not representative of the temperature in the corresponding cross section. Nevertheless, the deviation between the computational and experimental

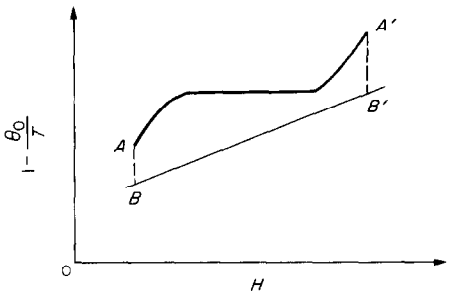

FIG. 14. Representation of the direct contact heat exchange thermodynamic transformation in the $[1-(\theta_0(T), H]$ plane.

results decreases with increasing continuous-phase flow rates. A higher continuous-phase Reynolds number (increasing turbulence...) allows better distribution of the dispersed phase in the continuous phase. In this case the assumptions made are more valid.

CONCLUSION

In this work, we have shown that direct contact heat exchangers with a liquid to solid change of state of the dispersed phase, are technically feasible. Their thermal characteristics are particularly well adapted to heat storage systems.

Volumetric heat transfer coefficients obtained are higher than those of classical exchangers (wall exchangers). Despite the complex phenomena involved, a model that satisfactorily interprets the heat exchanger was developed.

These exchangers present, however, certain problems:

—They require suitable couples which are immiscible and chemically inert.
—The dispersed-phase material may be swept along by the continuous phase according to the conditions flow.
—Exergetic efficiency is always less than unity due to the change of state and it is not improved by the counter-current flow mode.

REFERENCES

1. J. N. Solesio, Stabilité et métrologie des films liquides. Thèse de Doctorat es-sciences, Université scientifique et médicale et Institut national polytechnique de Grenoble (1978).
2. M. Antonini, G. Guiffant, J. P. Pain et P. Segaud, Mise au point d'un dispositif échangeur/stockeur à contact direct utilisant des paraffines contenerisées en nappes alvéolaires. Séminaire stockage thermique et sa modélisation, La Baule (1982).
3. T. L. Etherington and N. Y. Schenectady, A dynamic heat storage system, *Heat. Pip. Air Condit.* **29,** 147–151 (1957).
4. R. Letan and E. Kehat, The mechanism of heat transfer in a spray column heat exchanger, *A.I.Ch.E. Jl* 14, 398–405 (1968).
5. R. Deruaz, C. Lackme and A. Merle, Etude d'un échangeur à contact pour les dessalement de l'eau de mer. B.I.S.T. du CEA, No. 134 (1969).
6. D. E. Steinmeyer and C. E. Woodward, Liquid–liquid heat transfer in a large diameter spray column, *Chem. Engng Progr. Sympsoium ser.* No. 92, 65, 70–76 (1969).
7. S. Sideman and Y. Taitel, Direct contact heat transfer with change of phases: evaporation of drops in an immiscible liquid medium, *Int. J. Heat Mass Transfer* **7,** 1273–1289 (1964).
8. O. Favre, Contribution à l'étude d'un échangeur dynamique à contact direct par injection d'un sel fondu dans un fluide caloporteur. Thèse de Doctorat de Spécialité, Université de Provence (1978).
9. J. Pantaloni, O. Favre, R. Bailleux, G. Finiels et J. Marchisio, Stockage thermique de l'énergie par chaleur latente de fusion d'un sel minéral: Etude d'un échangeur dynamique à contact direct avec cristallisation du sel durant l'écoulement, *Revue Phys. appl.* **14,** 113 (1979).
10. J. Pantaloni et M. G. Velarde, Algunas cuestiones relatias al almacencemiento termico de la energia mediante sales fundidas, *Quim. Ind.* **22,** 778–783 (1976).
11. A. Bricard et B. Duret, Stockage thermique par chaleur de fusion. Système à contact direct. *Techq. Ingr.* **B269,** 5 (1981).
12. J. Pantaloni, M. Larini, H. Guenoche, M. Desaulty, J. Boyer, J. P. Petit et J. Huetz, Aperçu sur les possibilités de stockage thermique à haute température par chaleur latente, *Rev. Gén. Thermique France* No. 212–213 (1979).
13. M. Allibert, I. Ansara, A. Bricard, J. Chabanne et J. C. Poignet, Amélioration des performances de transfert d'un stockage de chaleur à contact direct à 500°C, Contrat DGRST, Décision d'aide No. 7971492.
14. P. Seguin, Réalisation, Etude et Modélisation d'un échangeur dynamique à contact direct sel fondu/huile couplé à un ensemble de stockage. Thèse de Docteur Ingénieur, Université de Provence (Marseille 1983).
15. Y. Coulibaly, Echangeur de chaleur à contact direct avec fluide intermédiaire á changement de phase liquide–solide. Thèse de Doctorat de 3e cycle, Institut National Polytechnique de Grenoble (1982).
16. A. Bricard et Y. Coulibaly, Echange par contact direct, Utilisation rationnelle de l'énergie. Colloque de Sophia Antipolis (1983).
17. R. E. Mugele and H. D. Evans, Droplet size distribution in spray, *Ind. engng Chem.* **43,** 1317 (1954).
18. B. Epstein, The mathematical description of certain breakage mechanisms leading to log-normal distribution. *J. Franklin Inst.* (Philadelphia, USA) **244,** 247 (1947).
19. R. Loutaty and M. Perrut, *Drop Size in a Liquid–Liquid Dispersion: Formation in a Jet Break-up.* Elsevier Sequoia, Lausanne (1971).
20. A. Putnam, F. Benningtoun and A. Battele, Injection and combustion of liquid fuels, Battele memorial Institute (1957).
21. L. Tadrist, Stockage d'énergie par chaleur latente: étude de la conductivité thermique des sels fondus. Etude d'un échangeur dynamique à contact direct huile-sel. Thèse de Doctorat de Spécialité Université de Provence, Marseille (1981).
22. S. B. Plass, H. R. Jacob and R. F. Boehn, Operational characteristics of a spray column type direct contact preheater. *A.I.Ch.E. Symposium Ser.* No. 189, **75,** 227–234 (1979).
23. M. Larini, Contribution à l'étude d'écoulements diphasiques. Thèse de Doctorat es-sciences, Université de Provence (1981).
24. M. Desaulty, Etude d'un échangeur à contre-courant gaz-gouttes de chlorure de sodium en cours de cristallisation, *Revue Phys. appl.* **15,** 189–199 (1980).
25. S. Ergun, Fluid flow through packed columns, *Chem. Engng Progr.* **48,** 49 (1952).
26. J. F. Richardson and W. D. Zaki, Sedimentation and fluidisation, *Trans. Inst. chem. Engrs* **32,** 37–53 (1954).
27. C. Bonacina and G. Comini, Numerical solution of phase change problems, *Int. J. Heat Mass Transfer* **16,** 1825–1832 (1973).

28. P. N. Rowe, K. T. Claxton and J. B. Lewis, Heat and mass transfer from a single sphere in an extensive flowing, *Trans. Inst. chem. Engrs* **43**, 14–31 (1965).
29. J. C. Chu, J. Kalil and W. A. Wetteroth, Mass transfer in a fluidized bed, *Chem. Engng Prog.* **49**, 141 (1953).
30. A. Markowitz and A. E. Bergler, Heat transfer in spray column, *Chem. Engng Progr. Symposium* Ser. No. 102, **66**, 63–71 (1970).
31. L. Moresco and E. Marshall, Liquid–liquid direct contact heat transfer in a spray column, *J. Heat Transfer* **102**, 684–687 (1980).
32. S. Hartland and J. C. Mecklenburgh, *Theory of Back Mixing*. Pergamon, Oxford (1973).
33. P. Le Goff, *Energétique Industrielle*, tome 1. Analyse thermodynamique et mécanique des économies d'énergie (edited by Lavoisier). Technique et documentation (1979).

ETUDE EXPERIMENTALE ET NUMERIQUE DES ECHANGEURS A CONTACT DIRECT

Résumé—Le présent papier porte sur l'étude des échangeurs de chaleur à contact direct avec changement de phase liquide–solide de la phase dispersée. L'expérimentation a porté sur deux systèmes ayant des points de fonctionnement différents. L'un Hitec/huile (T_{fonct} = 140°C), l'autre paradichlorobenzène/eau (T_{fonct} = 50°C). Nous montrons que la taille des particules en sortie de la colonne d'échange est une fonction des températures des phases dispersée et continue ainsi que la vitesse relative des deux fluides au niveau du disperseur. Parallèlement nous avons établi une modélisation globale basée sur l'évaluation de temps caractéristiques des transferts. Ceci a permis de corréler l'efficacité E à un nombre de Peclet caractéristique pour les échangeurs de ce type. Une modélisation plus fine a été réalisée en vue de prédire l'évolution des températures de chacune des phases le long de la colonne d'échange lorsque la répartition des particules est homogène dans l'échangeur. Les résultats du modèle sont comparés aux résultats expérimentaux.

EXPERIMENTELLE UND NUMERISCHE UNTERSUCHUNG VON DIREKTEN WÄRMETAUSCHERN

Zusammenfassung—Diese Arbeit ist eine Studie über einen direkten Wärmetauscher zwischen Flüssigkeit und Feststoff. Die Experimente wurden an zwei Systemen bei unterschiedlichen Arbeitstemperaturen durchgeführt: 'Hitec'/Öl (bei 140°C), Paradichlorbenzol/Wasser (bei 50°C). Die Verteilung der Teilchengröße am Austritt der Wärmetauschersäule ist sowohl eine Funktion der Temperatur der dispersen und der kontinuierlichen Phase als auch der relativen Geschwindigkeiten der beiden Fluide an der Düse. Wir haben ein Modell entwickelt, das die für die Wärmeübertragung charakteristischen Zeiten zugrundelegt: Es gibt eine Beziehung zwischen dem Wärmetauscher-Wirkungsgrad und der charakteristischen Peclet-Zahl für diese Art von Wärmetauschern. Wir entwickelten ein weiteres Modell für die Wärmeübertragung innerhalb der Zweiphasenströmung, welches das Temperaturprofil der kontinuierlichen Phase entlang der austauschenden Säule und den Wirkungsgrad des Wärmetauschers angibt. Die Ergebnisse dieses Modells wurden mit den experimentell erhaltenen verglichen.

ЭКСПЕРИМЕНТАЛЬНОЕ И ЧИСЛЕННОЕ ИССЛЕДОВАНИЕ КОНТАКТНЫХ ТЕПЛООБМЕННИКОВ

Аннотация—В работе изучается контактный теплообменник с фазовым переходом жидкость–твердое вещество. Эксперименты проводились на двух системах с различными рабочими температурами: хитек/масло (при 140°C) и парадихлорбензол/вода (при 50°C). Распределение частиц по размерам на выходе из колонны теплообменника является функцией температур дисперсной и непрерывной фазы, а также их относительной скорости на срезе у сопла. Создана модель, основанная на характерных временах теплообмена. Для данного типа теплообменников получено отношение их эффективности к характерному числу Пекле. Предложена также модель теплообмена внутри двухфазного течения, дающая профиль температуры непрерывной фазы вдоль колонны теплообменника и его эффективность. Результаты численного моделирования сравниваются с экспериментальными данными.